# Evaluation of South African Candidate Sites for an Expanded Event Horizon Telescope

*Senkhosi Simelane, Roger Deane, Athol Kemball, Roelf Botha, Roufurd Julie, Keitumetse Molamu, Adrian Tiplady, and Aletha de Witt*

*Abstract* – Global expansion of the Event Horizon Telescope (EHT) will see the strategic addition of antennas at new geographic locations, transforming the sensitivity and imaging fidelity of the $\lambda \sim 1$-mm EHT array. A possible South African EHT station would leverage a strong geographic advantage, local infrastructure, and radio astronomy expertise and have strong synergies with the Africa Millimetre Telescope in Namibia. We assessed three South African candidate millimeter sites using climatologic simulations and antenna sensitivity estimates and found at least two promising sites. These sites are comparable to some existing EHT stations during the typical April EHT observing window and outperform them during most of the year, especially the southern hemisphere winter. The results suggest that a strategically placed South African EHT station will have a sizable, positive impact on next-generation EHT objectives and the resulting black hole–imaging science.

## 1. Introduction

A host of novel black hole (BH) science goals will be enabled by the expansion of the Event Horizon Telescope (EHT) [1, 2], including the reconstruction of high-fidelity movies of the Messier 87* (M87*) and Sagittarius A* (Sgr A*) supermassive BHs (SMBHs). Both sources display dynamic behavior, with timescales of approximately 20 days [3] and approximately 20 minutes [4–6], respectively. However, the typical 1-week duration of EHT observing campaigns is too short to capture the full dynamical evolution of M87*, [7] and limited snapshot $(u, v)$ coverage has meant that the rapid time variability of Sgr A* remains poorly constrained [8]. These limitations have precluded experiments that allow dynamic imaging of SMBHs. New, strategically placed stations, especially several on the African continent, would extend the annual monitoring window for M87* and also significantly improve the instantaneous and full-track $(u, v)$ coverage toward Sgr A* [9, 10], while prompting significant strides in African Very Long Baseline Interferometry (VLBI) development, particularly with intra-African VLBI baselines.

Southern Africa holds a strong geographic advantage for imaging southern hemisphere sources, such as Sgr A*. Simulations by [10] showed that adding the Africa Millimetre Telescope (AMT) in Namibia and a Canary Islands station to the EHT improves Sgr A* movie fidelity through better constraints on source extent and a factor $\gtrsim 4$ increase in observation length with adequate snapshot $(u, v)$ coverage for dynamical imaging. Static Sgr A* imaging from [9] showed that an EHT array augmented with the AMT and a South African station achieves significantly improved $(u, v)$ coverage, especially in the eastern subarray. Through long north-south and east-west baselines to NOEMA and ALMA, respectively, a South African EHT station (SA-EHT hereafter) would further enhance dynamical reconstructions of Sgr A* and M87* and potentially enable polarimetric photon ring experiments, as proposed by [11]. Additionally, a short ($\sim$1000 km) SA-EHT-AMT baseline would enable the measurement of low-spatial-frequency emission critical for linking jet launch with horizon-scale dynamics. The added short-baseline constraints would also improve the gain calibration solutions and hence the achieved image fidelity [12] and dynamic range, particularly with maximum entropy method imaging [13].

The prospective array of performance improvements offered by the addition of SA-EHT to the EHT strongly motivate an investigation of feasible millimeter sites in South Africa. To this end, three sites were identified for preliminary evaluation, including Ben Macdhui (BMAC) in South Africa's Eastern Cape, Sutherland (STL) in the Northern Cape, and Matjiesfontein (MATJ) in the Western Cape. Details of the sites, selected for their relatively high altitude and existing infrastructure, are summarized in Table 1. The preselection criterion for sites to have existing infrastructure is motivated by a more rapid and cost-effective SA-EHT project delivery.

Tropospheric water vapor is the chief cause of atmospheric absorption and scattering of millimeter waves, necessitating high-altitude, low-humidity sites. The frequency-dependent absorption, quantified by the optical depth, $\tau(\nu)$, attenuates incoming millimeter radiation as $e^{-\tau(\nu)}$ and a fast-evolving water vapor distribution above a millimeter station causes rapid phase fluctuations. The coherence time, defined as the mean time interval over

Manuscript received 29 October 2024.

Senkhosi Simelane and Roger Deane are with the Wits Centre for Astrophysics, School of Physics, University of the Witwatersrand, 1 Jan Smuts Avenue, Johannesburg, Gauteng 2000, South Africa; e-mail: senkhosi.simelane1@students.wits.ac.za, roger.deane@wits.ac.za.

Athol Kemball is with the Department of Astronomy, University of Illinois Urbana-Champaign, 1002 W. Green St, Urbana, Illinois 61801, United States of America; e-mail: akemball@illinois.edu.

Roelf Botha, Roufurd Julie, Keitumetse Molamu, and Adrian Tiplady are with the South African Radio Astronomy Observatory, River Park Liesbeek Parkway, Settlers Way, Cape Town, Western Cape 7705, South Africa; e-mail: rbotha@sarao.ac.za, rjulie@sarao.ac.za, kmolamu@sarao.ac.za, atiplady@sarao.ac.za.

Aletha de Witt is with the Department of Science and Innovation, 671 Meiring Naudé Road, Pretoria, Gauteng 0184, South Africa; e-mail: aletha.dewitt@dst.gov.za.

Table 1. Geographic information of the following three SA-EHT candidate sites: Ben Macdhui (BMAC), Sutherland (STL) and Matjiesfontein (MATJ)

| Site | Latitude, deg | Latitude, deg | Altitude, m |
|---|---|---|---|
| Ben Macdhui | −30.648 | 27.935 | 3000 |
| Sutherland | −32.378 | 20.813 | 1800 |
| Matjiesfontein | −33.266 | 20.582 | 1340 |

which the troposphere induces a 1-radian phase shift, characterizes the rate of these fluctuations. Thus, the column-integrated precipitable water vapor (PWV) and $\tau(\nu)$ are key parameters in millimeter site evaluations. For the next-generation EHT (ngEHT), the 86, 230, and 345-GHz zenith optical depths are of the most interest as these align with the proposed receiver bands [2]. Wind speeds are also critical, as high wind speeds degrade coherence times, disrupt dish pointing and tracking, and may even necessitate stowing of the dish. This work evaluated these climatologic proxies, among others, and used them to estimate antenna sensitivity for various dish sizes via the system equivalent flux density (SEFD). This analysis marks a first step toward identifying an SA-EHT dish size that offers the best value proposition while delivering significant scientific impact.

The work is presented as follows: the methods employed in the climatologic site characterization and antenna sensitivity estimation study are presented in Sections 2 and 3. The results are presented and discussed in Section 4. Finally, Section 5 summarizes the key results and gives an outlook on the next steps and outstanding questions.

## 2. Climatologic Modeling

To characterize the candidate SA-EHT sites, we employed a meteorological modeling approach akin to [14–17]. Using data from Modern-Era Retrospective Analysis for Research and Applications, version 2 (MERRA-2) [18], a global database of atmospheric measurements on a 0.5° latitude by 0.625° longitude (or ∼55 km latitude by ∼70 km) grid from 1980 to date, we generated realistic model atmospheres. MERRA-2 has a 3-hour temporal resolution, but a temporal resolution of 1 month was used for this analysis as it suffices for the goal of shortlisting sites for on-site testing. We used daily MERRA-2 data files from January 1, 2009, to December 31, 2022, to calculate monthly means of the quantities needed for model atmosphere generation, which we then used to create model atmospheres.

In the absence of on-site air pressure measurements, we devised a surface pressure estimation approach requiring only the site latitude, $S_{lat}$, longitude, $S_{lon}$ and altitude (height above sea level) $S_{alt}$ as inputs. The method employs the MERRA-2 vertical pressure levels, *lev*, and the mean edge heights, $H$, the mean altitudes to which they correspond, from the surrounding grid points. For each grid point, the closest mean edge heights above and below $S_{alt}$ are determined, the corresponding pressure levels identified, and a linear interpolation between the pair of points is carried out to estimate the pressure at the height $S_{alt}$. The

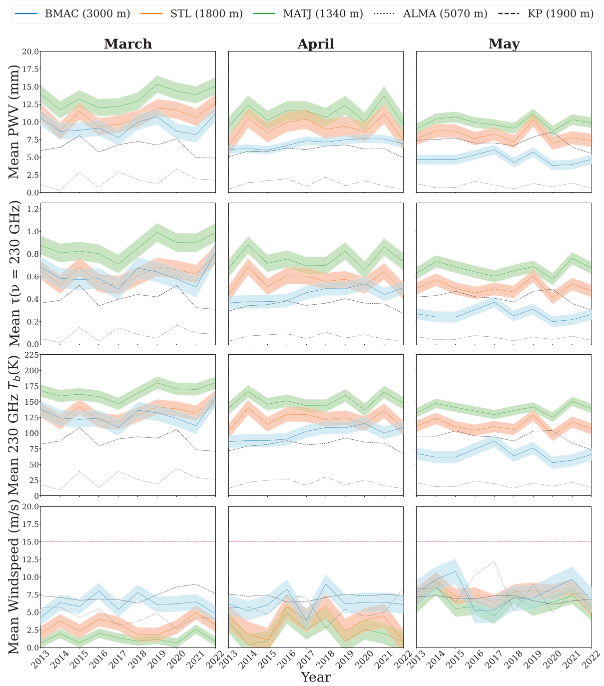


Figure 1. Monthly mean PWV (top row), 230-GHz zenith opacity (second row) and brightness temperature (third row), and wind speed (bottom row) above BMAC, STL, and MATJ for March, April, and May from 2013-2022. Predictions for BMAC, STL, and MATJ are shown by blue, orange, and green curves, respectively, with shaded regions indicating $\pm\sigma$. Means plus $\sigma$ above KP (dashed) and means minus $\sigma$ above ALMA (dotted) contextualize the SA-EHT values within the typical range of atmospheric conditions in the array. The dashed magenta line (bottom row) marks a wind speed of 15 m/s.

estimated pressures at $S_{alt}$ from the four grid points are then interpolated bilinearly to estimate the surface pressure, $P_{surf}$, at the site location, ($S_{lat}$, $S_{lon}$, $S_{alt}$). Finally, the mean vertical profiles of other quantities [17, fig. 1] are determined by bilinearly interpolating the mean MERRA-2 profiles of the surrounding grid points to ($S_{lat}$, $S_{lon}$), truncating the profiles at the closest vertical pressure level above $S_{alt}$ and using $P_{surf}$ to logarithmically extrapolate them to ($S_{lat}$, $S_{lon}$, $S_{alt}$). To avoid negative wind speed predictions, wind speeds were instead estimated by linearly interpolating between the values at the pressure levels closest to $P_{surf}$ above and below.

Following atmospheric model generation, we used the am atmospheric modeling software [19] to solve the radiative transfer equation for the models, effectively estimating ground-based radiometer measurements by simulating the effect of atmospheric absorption, emission, and scattering on radio frequency signals passing through the model atmospheres. We chose a frequency range of 80 to 700 GHz with 500-MHz resolution. Estimated quantities include the mean PWV, zenith optical depth $\tau(\nu)$, zenith brightness temperature $T_b(\nu)$, and wind speed $v_{wind}$.

## 3. Sensitivity Estimation

Equipped with the $\tau(\nu)$ and $T_b(\nu)$ values, we estimated the effective sensitivity of the antenna and receiver at 230 GHz through single-dish SEFDs for different dish diameters using the definition [20]

$$\mathrm{SEFD} \equiv \frac{2k_\mathrm{B}T_\mathrm{sys}}{\eta A_\mathrm{geo}}.$$

In the equation above, $k_\mathrm{B}$ is the Boltzmann constant, $T_\mathrm{sys}$ the absorption-corrected system temperature, $A_\mathrm{geo}$ the geometric area of the dish and $\eta$ an efficiency factor encapsulating all relevant effects. Assuming a perfectly sideband-separating receiver system, we calculated $T_\mathrm{sys}$ as

$$T_\mathrm{sys}(\nu) = e^{\tau(\nu)}[T_\mathrm{rec}(\nu) + (1 - e^{-\tau(\nu)})T_\mathrm{atm}(\nu)],$$

where $T_\mathrm{rec}(\nu)$ is the receiver temperature and $T_\mathrm{atm}(\nu)$, the effective atmospheric temperature, is

$$T_\mathrm{atm}(\nu) = \frac{T_b(\nu) - T_\mathrm{CMB}e^{-\tau(\nu)}}{1 - e^{-\tau(\nu)}}.$$

We assumed the ALMA 230-GHz receiver temperature of $T_\mathrm{rec} = 40$ K [17, table 5] and $T_\mathrm{CMB} = 2.725$ K [21]. Our $\eta$ estimates considered only the forward efficiency and aperture efficiency:

$$\eta(\nu) = \eta_\mathrm{F}(\nu)\eta_\mathrm{ap}(\nu).$$

We chose $\eta_\mathrm{F} = 0.9$ for all sites, which is similar to values adopted in other EHT expansion analyses [17]. The aperture efficiency, $\eta_\mathrm{ap}$, was calculated using Ruze's formula [22], assuming a focus offset of 10 μ m and a commercially available dish with an RMS surface accuracy of 40 μ m.

These calculations underpin the 230-GHz noise performance analysis of hypothetical dishes at the candidate sites in Section 4, incorporating dish and receiver specifications and the site-specific atmospheric conditions calculated in Section 2. Three indicative dish diameters (9, 13, and 18 m) were included based on ngEHT and next-generation Very Large Array designs.

## 4. Results and Discussion

We validated the climatologic characterization results through comparison with BMAC weather data from the ngehtsim package, which was the only South African candidate site whose weather data was included in [15] and ngehtsim [17]. The results were consistent, yielding mean relative differences of approximately 4%, approximately 9%, and approximately 17% for the mean 230-GHz zenith optical depth, mean PWV, and mean wind speed, respectively, which are lower than the RMS of each parameter. With the validation completed, the analysis of all three candidate SA-EHT sites was undertaken.

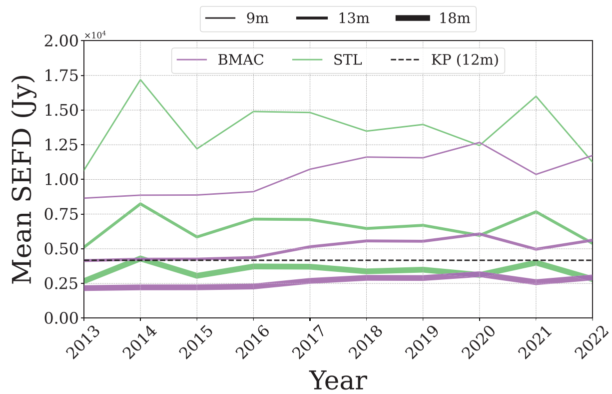


Figure 2. Mean SEFD estimates for different dish sizes during the month of April from 2013 to 2022. Thicker linewidths correspond to large dish diameters at two South African sites, BMAC (purple) and STL (green). A black, dashed horizontal line at the mean value of KP over the decade is added for context. Values generally showed a standard deviation of approximately 3000 Jy.

### 4.1 Nominal EHT Observing Window Comparison

Over the decade analyzed, BMAC generally exhibited the lowest mean PWV values among the three South African sites. As an EHT site located at a relatively low altitude of 1900 m, Kitt Peak (KP) has some of the least favorable millimeter observing conditions in the array. Thus, we used it as a benchmark nonpremier site against which to evaluate the SA-EHT candidate sites. In April, the customary EHT observing window, the mean PWV, and the 230-GHz optical depths and brightness temperatures above BMAC are comparable to those above KP (see middle column of Figure 1), a pattern also observed at 86 and 345 GHz. While STL's mean PWV, $\tau(\nu)$, and $T_b(\nu)$ curves approach those of BMAC during certain years, the STL and MATJ curves generally exceed the upper bound of the KP 1-standard-deviation ($\sigma$) range. In May, BMAC's curves fall well below KP + $\sigma$, while those of STL remain close to them. The ~10-mm conditions at BMAC and STL in March decline to ~5 mm (STL) and $<$ 5 mm (BMAC) from April through August, representing an important trend as the ngEHT project seeks to extend the observing window to ~3 months in Phase 1 [2].

Similar wind speeds to STL and MATJ during the first half of the year and significantly higher values during the latter half make BMAC the windiest site of the three. Wind-induced sensitivity degradation depends on antenna specifications, but at wind speeds less than 15 m/s, degradation is typically insubstantial [17]. The mean wind speeds at all three candidate SA-EHT sites rarely reach this mark. We note, however, that the MERRA-2 data lack the time resolution to capture gusting. This is left for future analysis of on-site measurements.

We explored 9, 13 and 18-m dish diameters in our estimated sensitivity analysis. The hypothetical 13-m dish at BMAC and 18-m dish at STL showed mean SEFDs similar to those of the KP antenna in April (see Figure 2). Specifically, KP marginally outperforms a BMAC

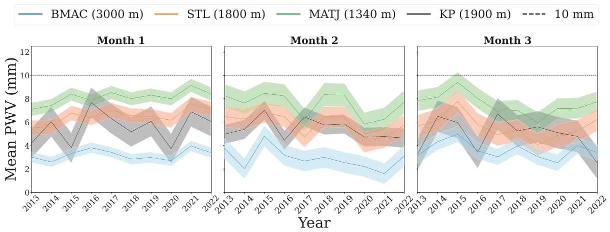


Figure 3. Winter monthly mean PWV above BMAC, STL, MATJ, and KP from 2013-2022. Predictions for BMAC, STL, MATJ, and KP are shown by blue, orange, green, and black curves, respectively, with shaded regions indicating $\pm\sigma$. The dashed black line marks a PWV of 10 mm.

13-m dish and is marginally outperformed by an STL 18-m dish, reflecting KP's slightly superior April 230-GHz zenith opacities and brightness temperatures. The noise performance difference between BMAC and STL diminishes with increasing dish diameter. While an 18-m dish at BMAC outperforms the same dish at STL, the difference is minimal during the latter half of the decade analyzed, partly due to an apparent uptrend in April brightness temperatures and zenith opacities at BMAC. This trend warrants further monitoring with a MERRA-2 data subset that includes data for 2023 and 2024.

### 4.2 Winter–Winter Comparison

The goal of achieving year-round observations in Phase 2 of the ngEHT project [2] relaxes the requirement of sub-10 mm PWV conditions specifically around April, allowing a broader assessment of site quality across seasons. This enables us to remove the effect of opposing seasonal patterns between the southern and northern hemispheres by comparing the quality indicators of the candidate SA-EHT sites and KP during equivalent seasonal periods. Since winter observing conditions are generally more favorable than summer conditions, we focused on the meteorological winters as follows: June 1 to August 31 in the southern hemisphere and December 1 to February 28/29 in the northern hemisphere. Figure 3 demonstrates that STL and KP offer similar site quality for millimeter observations, while the higher-altitude BMAC site exhibits conditions superior to both. Typically, falling below the 10-millimeter mark in the same figure, all three SA-EHT candidate sites become competitive millimeter sites in the southern hemisphere winter. Notably, only in March and the period plotted in Figure 3 do KP's mean PWVs and zenith spectral opacities consistently suggest more favorable conditions than BMAC and STL. Furthermore, observing conditions at the South African sites are relatively stable throughout the year. For instance, PWV values above KP deteriorate by a factor greater than 6 (to $\sim$30 mm in July and August) in the northern hemisphere summer compared with April, while even the MATJ PWV values seldom exceed 15 mm. This stability is significant for year-round observing and opens the door to southern-winter VLBI observations with the AMT and Atacama Desert stations (ALMA and APEX), particularly with Frequency Phase Transfer (FPT)-enabled stations.

## 5. Conclusion

Among the three candidate SA-EHT sites selected for desktop evaluation, BMAC showed the most promising proxies for millimeter site quality, comparable to KP during the nominal April EHT observing window and outperforming it during most of the year. In its most favorable years, however, STL's weather conditions are similar to those of BMAC in this window, and it is comparable to KP when the sites' weather conditions are compared for similar meteorologic seasons. In our view, BMAC and STL justify the financial investment of in situ characterization.

The positive millimeter site quality and antenna sensitivity indicators emphasize the importance of the next steps. FPT will very likely play a pivotal role in future EHT operations, particularly at nonpremier sites. It is, therefore, also important to incorporate this technique in an extension of this study to static and dynamical imaging, especially characterizing its performance as a function of sensitivity to help inform the recommended SA-EHT dish size.

## 6. Acknowledgements

The authors thank Lindy Blackburn, Iniyan Natarajan, Daniel Palumbo, and Dominic Pesce for insightful discussions that greatly benefitted this work. They are especially grateful to Dominic Pesce for adding their candidate sites to ngehtsim, which significantly streamlined the analysis, and also appreciate the constructive feedback from two anonymous referees.

## 7. References

1. M. D. Johnson, K. Akiyama, L. Blackburn, K. L. Bouman, A. E. Broderick, et al., "Key Science Goals for the Next-Generation Event Horizon Telescope," *Galaxies*, **11**, 3, April 2023, p. 61.
2. S. S. Doeleman, J. Barrett, L. Blackburn, K. L. Bouman, A. E. Broderick et al., "Reference Array and Design Consideration for the Next-Generation Event Horizon Telescope," *Galaxies*, **11**, 5, October 2023, p. 107.
3. G. C. Bower, J. Dexter, S. Markoff, M. A. Gurwell, R. Rao, et al., "A Black Hole Mass-Variability Timescale Correlation at Submillimeter Wavelengths," *Astrophys J Lett*, **811**, 1, 2015, L6.
4. R. Genzel, R. Schödel, T. Ott, A. Eckart, T. Alexander et al., "Near-infrared flares from accreting gas around the supermassive black hole at the Galactic Centre," *Nature*, **425**, 6961, 2003, pp. 934-937.
5. A. M. Ghez, S. A. Wright, K. Matthews, D. Thompson, D. Le Mignant et al., "Variable Infrared Emission From the Supermassive Black Hole at the Center of the Milky Way," *Astrophys J*, **601**, 2, 2004, L159.
6. R. Abuter, A. Amorim, M. Baubock, et al.; for the Gravity Collaboration et al, "The Flux Distribution of Sgr A," *Astron Astrophys*, **638**, June 2020, A2.
7. Event Horizon Telescope Collaboration, K. Akiyama, A. Alberdi, W. Alef, K. Asada, et al., "First M87 Event Horizon Telescope Results. V. Physical Origin of the Asymmetric Ring," *Astrophys J Lett*, **875**, 1, Apr 2019, L5.
8. Event Horizon Telescope Collaboration, K. Akiyama, A. Alberdi, W. Alef, Algaba J. C., et al., "First Sagittarius A*

Event Horizon Telescope Results. I. The Shadow of the Supermassive Black Hole in the Center of the Milky Way," *Astrophy J Lett*, **930**, 2, May 2022, L12.

9. R. Deane and I. Natarajan, "The First Image of the Milky Way's Central Black Hole and the Unique Enhancement Africa Could Offer Future Tests of Gravity," *S Afr J Sci*, **118**, 7-8, July 2022, pp. 1-4.
10. N. La Bella, S. Issaoun, F. Roelofs, C. Fromm, and H. Falcke, "Expanding Sgr A* Dynamical Imaging Capabilities with an African Extension to the Event Horizon Telescope," *Astron Astrophys*, **672**, April 2023, A16.
11. D. C. M. Palumbo, G. N. Wong, A. Chael, and M. D. Johnson, "Demonstrating Photon Ring Existence with Single-baseline Polarimetry," *Astrophys J Lett*, **952**, 2, August 2023, L31.
12. T. Cornwell and E. B. Fomalont, "Self-Calibration," in G. B. Taylor, C. L. Carilli, and R. A. Perley (eds.), *Synthesis Imaging in Radio Astronomy II.* Orem, Astronomical Society of the Pacific Conference Series, 1999, pp. 187-199.
13. R. Narayan and R. Nityananda, "Maximum Entropy Image Restoration in Astronomy," *Annual Rev Astron Astrophys*, **24**, 1986, pp. 127-170.
14. F. Roelofs, M. Janssen, I. Natarajan, R. Deane, J. Davelaar, et al., "SYMBA: An End-to-End VLBI Synthetic Data Generation Pipeline - Simulating Event Horizon Telescope Observations of M 87," *Astron Astrophys*, **636**, April 2020, A5.
15. A. W. Raymond, D. Palumbo, S. N. Paine, L. Blackburn, R. Córdova Rosado, et al., "Evaluation of New Submillimeter VLBI Sites for the Event Horizon Telescope," *The Astrophys J Suppl Ser*, **253**, 1, March 2021, p. 5.
16. W. Yu, R. S. Lu, Z. Q. Shen, and J. Weintroub, "Evaluation of a Candidate Site in the Tibetan Plateau Towards the Next Generation Event Horizon Telescope," *Galaxies*, **11**, 1, February 2023, p. 7.
17. D. W. Pesce, L. Blackburn, R. Chaves, S. S. Doeleman, M. Freeman et al., "Atmospheric Limitations for High-Frequency Ground-Based VLBI," *arXiv e-prints*, April 2024, arXiv: 2404.01482.
18. R. Gelaro, W. McCarty, M. J. Suárez, R. Todling, A. Molod, et al., "The Modern-Era Retrospective Analysis for Research and Applications, Version 2 (MERRA-2)," *J Clim*, **30**, 14, 2017, pp. 5419-5454.
19. S. Paine, "The am Atmospheric Model," *Zenodo*, version 11.0, https://zenodo.org/records/3406496, 2019.
20. G. B. Taylor, C. L. Carilli, and R. A. Perley, *Synthesis Imaging in Radio Astronomy II*, Orem, Astronomical Society of the Pacific Conference Series, 1999.
21. J. C. Mather, D. J. Fixsen, R. A. Shafer, C. Mosier and D. T. Wilkinson, "Calibrator Design for the COBE* Far Infrared Absolute Spectrophotometer (FIRAS)," *Astrophys J*, **512**, 2, February 1999, p. 511.
22. J. Ruze, "Antenna Tolerance Theory – A Review," *Proc IEEE*, **54**, 4, April 1966.